Pt Electrocatalysts

DOI: 10.1002/anie.201201553

Self-Supported Interconnected Pt Nanoassemblies as Highly Stable Electrocatalysts for Low-Temperature Fuel Cells

Bao Yu Xia, Wan Theng Ng, Hao Bin Wu, Xin Wang, and Xiong Wen (David) Lou**

Low-temperature fuel cells have attracted considerable attention because of their high power density, low operating temperature (< 120 °C), and reduced pollution as a new power source for automobiles and portable electronic devices.[1,2] However, their commercialization is impeded by the poor durability and activity of electrocatalysts.[2–4] State-of-the-art electrocatalysts primarily consist of Pt nanoparticles (NPs) supported on carbon black (Pt/CB).[5] The poor durability of Pt/CB catalysts is reflected in a fast and significant loss of electrochemical surface area (ECSA) and thus degradation of the fuel cells performance. It has been argued that the loss of ECSA is mainly ascribed to the corrosion of carbon supports, which further results in migration, aggregation, and Ostwald ripening of Pt NPs because of their high surface energy and zero-dimensional (0D) structural features.[6,7]

One effective strategy to improve the durability of electrocatalysts is to use one-dimensional (1D) Pt nanostructures, including nanowires (NWs),[8,9] nanorods,[10,11] and nanotubes,[12,13] owing to their inherent anisotropic morphology and unique structure compared to the isotropic 0D Pt NPs.[14–16] Meanwhile, the 1D Pt nanostructures have a unique combination of dimensions in multiple length scales, and they do not require a high surface-area support (e.g. carbon black). Thus, they have the potential to avoid the carbon-corrosion problem and further improve mass-transport characteristics.[13,17] Nevertheless, most of the reported 1D Pt nanocatalysts are in the form of freestanding nanocrystals, which are similar to the Pt/CB catalyst.[18] Recently, assembly of 1D nanostructured Pt into two-dimensional (2D) membranes[18] and even three-dimensional (3D) nano-networks[19,20] has attracted remarkable attention because of their many unique structural characteristics, including high porosity, good flexibility, large surface area per unit volume, and interconnected open-pore structures.[20,21] Thus, the synthesis of controlled NW assembly would be an important new development, because each individual NW can be connected with a number of NWs in different ways to provide a large diversity of interconnectivity.[19,22,23] Consequently, the many efforts devoted to this area have led to 3D NW superstructures, such as arrays,[24–26] networks,[19] and hierarchical structures.[27] Compared with template-assisted strategies for nanoassemblies,[19,20,28] however, it is significantly more challenging to develop a direct synthesis approach for 3D nanoassemblies.[29–31]

Herein, we report the synthesis, characterization, and electrochemical evaluation of Pt nanoassemblies prepared by a one-pot method (see Supporting Information for the experimental details). We found that each Pt nanoassembly contained more than ten interconnected Pt NWs. This structure could maximize the surface area to volume ratio and therefore decrease the amount of catalytically inactive support material, while simultaneously minimizing the loading of the precious metal.[7,32] Moreover, the interconnected 3D nanoassemblies, consisting of long nanowires, make the Pt less vulnerable to dissolution, migration, Ostwald ripening, and aggregation compared to the 0D Pt nanoparticles. Furthermore, the mass transfer within the electrode can be facilitated by building 3D porous structures with the anisotropic, interconnected Pt NWs. Because of their many advantages, such 3D Pt-nanoassembly catalysts exhibit higher durability and activity than commercial electrocatalysts made of CB-supported 0D Pt nanoparticles.

Figure 1a shows a representative field-emission scanning electron microscopy (FESEM) image of Pt nanoassemblies. The as-prepared Pt nanoassemblies were of high uniformity and each nanoassembly was composed of many long Pt NWs. It is interesting that the Pt NW subunits point out in various directions to form the 3D hierarchical structure. X-ray diffraction (XRD) and energy dispersive X-ray (EDX) analyses confirmed that the as-prepared samples consisted exclusively of Pt (Supporting Information, Figure S1 and S2) with a face-centered cubic (fcc) structure (JCPDS card no. 04-0802). The morphology and structure of the nanoassemblies were further characterized by transmission electron microscopy (TEM). An overview TEM image of Pt nanoassemblies is shown in Figure 1b, displaying that each 3D Pt nanoassembly contained about 8–15 Pt NWs. The diameter and length of the Pt NWs were in the range of 5–10 nm and 100–200 nm, respectively, corresponding to an aspect ratio of about 20. The selected-area electron-diffraction (SAED) pattern (inset of Figure 1b) of Pt nanoassemblies showed concentric rings, composed of bright discrete diffraction spots, that were indexed to (111), (220), (311), and (331) crystal planes of fcc Pt, indicating the high degree of crystallinity of individual NWs. A TEM image with high magnification of a single Pt nanoassembly is shown in Figure 1c. We clearly

[*] Dr. B. Y. Xia, W. T. Ng, H. B. Wu, Prof. X. Wang, Prof. X. W. Lou
School of Chemical and Biomedical Engineering, Nanyang Technological University
70 Nanyang Drive, Singapore 637457 (Singapore)
E-mail: wangxin@ntu.edu.sg
xwlou@ntu.edu.sg
Homepage: http://www.ntu.edu.sg/home/xwlou
Dr. B. Y. Xia, Prof. X. W. Lou
Energy Research Institute @ NTU, Nanyang Technological University
50 Nanyang Drive, Singapore 637553 (Singapore)

Supporting information for this article (experimental details) is available on the WWW under http://dx.doi.org/10.1002/anie.201201553.

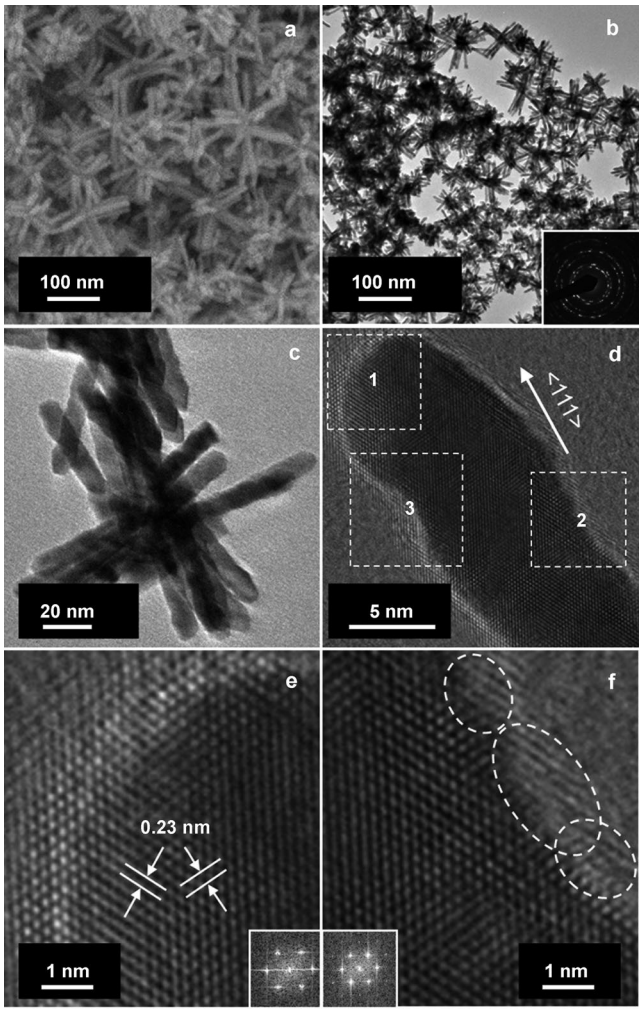

Figure 1. a) Representative FESEM and b) TEM images of the interconnected Pt nanoassemblies. Inset of (b): SAED pattern of Pt nanoassemblies. c) TEM image of a single Pt nanoassembly consisting of NWs. d) HRTEM micrograph of a single-crystalline Pt NW, with the direction of growth along the ⟨111⟩ axis; e, f) the magnified HRTEM micrographs recorded from regions 1 and 2 marked in (d), respectively. Insets of (e, f): corresponding FFT patterns.

observed that the Pt nanoassembly consists of about 15 Pt NWs that are approximately 10 nm in diameter and 200 nm in length. More interestingly, these NWs are interconnected at the center. This pattern suggests that the formation of a Pt nanoassembly might involve growth from a common point rather than the simple aggregation of preformed particles.[33] The detailed structural features of the NWs were characterized by high-resolution TEM (HRTEM), as shown in Figure 1 d. HRTEM observation of a Pt NW revealed the single-crystal nature of the NW, with a growth direction along the ⟨111⟩ axis. The lattice spacing of 0.23 nm (Figure 1 e) corresponded well to the interplane spacing of Pt (111) planes. Furthermore, the Pt NW had a step or concave surface topology and high-index exposed facets as marked in Figure 1 f, as well as in regions 1 and 3 in Figure 1 d. The fast Fourier transform (FFT) patterns of the atomic lattice fringes were identical, as displayed in the insets of Figure 1 e, f, further showing the single crystallinity of the NW along the ⟨111⟩ direction. These highly crystalline Pt nanoassemblies, consisting of interconnected Pt NWs, are believed to be a good candidate for fuel-cell catalysts.

To study the mechanism of 3D Pt nanoassembly formation from interconnected 1D Pt NWs, the roles of synthesis reagents were investigated in detail. It was previously reported that oleylamine could facilitate the formation and growth of Pt NWs/nanorods.[34] In the present synthesis system, oleylamine serves simultaneously as the solvent, reducing agent, and stabilizer for the formation of metal nanostructures.[8] Oleylamine might act as a ligand to form stable Pt^{4+} complexes and lead to the reduction of Pt^{4+} complexes to a metallic state at an elevated temperature.[29] Additionally, cetyltrimethylammonium bromide (CTAB) might play an important role as the structure-directing agent in the formation of multi-wire structures.[35] Only irregular multipods were obtained without the addition of CTAB (Figure 2 a). When the amount of CTAB was increased to 50 mg, the desired 3D Pt nanoassemblies containing interconnected Pt NWs were formed. Further increasing the amount of CTAB (100 mg) resulted in the formation of Pt nanoassemblies composed of many short nanorods. This result suggests that the interconnected Pt networks are likely to form only in the presence of CTAB.[36] The evolution of the morphology with reaction time has also been studied to understand the formation of Pt nanoassemblies. As revealed by the FESEM and TEM images in Figure S3 (see Supporting Information), the length of constituent Pt NWs increased as the reaction progressed. This observation suggests that the slow reduction of Pt^{4+} ions in oleylamine solution, in the presence of CTAB, favors the growth of Pt nanocrystals along the ⟨111⟩ direction and thereafter the formation of hierarchical nanoassemblies.

We next evaluated the electrocatalytic activity of the Pt nanoassemblies for the oxygen-reduction reaction (ORR). This test is conducted in an O_2-saturated 0.5 M H_2SO_4 solution using a glassy carbon (GC) rotation disk electrode (RDE) at room temperature with a sweep rate of 10 mV s^{-1}. Figure 3 a shows the ORR polarization curves for Pt nanoassemblies, commercial Pt electrocatalyst (E-TEK, 50 wt % Pt), and self-prepared Pt/CB (20 wt % Pt; see Supporting Information, Figure S4 and S5 for XRD/TEM characterizations of commercial Pt and Pt/CB). The half-wave potentials of Pt nanoassemblies, commercial Pt, and Pt/CB were 0.839, 0.829, and 0.818 V, respectively, showing that the activity of

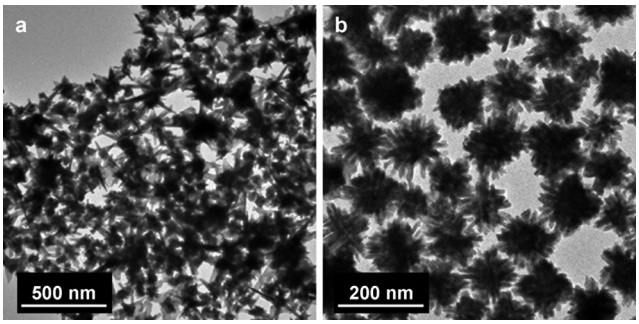

Figure 2. TEM images of Pt nanoassemblies prepared with or without CTAB: a) 0; b) 100 mg CTAB.

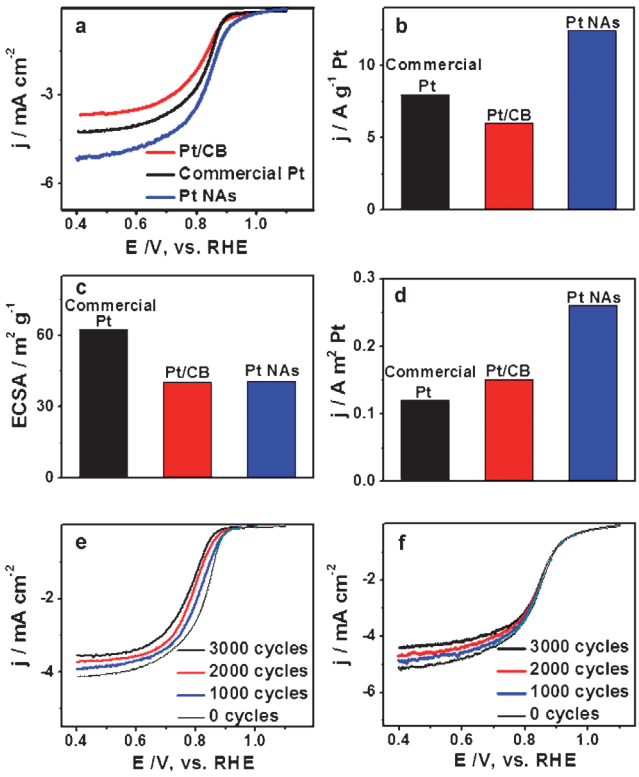

Figure 3. a) Polarization curves for ORR of Pt nanoassemblies (NAs), commercial Pt and Pt/CB in an O_2 saturated 0.5 M H_2SO_4 solution at room temperature (1600 rpm; sweep rate: 10 mV s^{-1}). j = current density. b) Mass activity (at 0.85 V vs. RHE), c) ECSA, and d) specific activity for the three catalysts. The polarization curves were obtained after different numbers of cycles for commercial Pt (e) and Pt nanoassemblies (f).

the Pt nanoassemblies was higher than that of commercial Pt and Pt/CB catalysts. Mass activity and specific activity are important parameters of electrocatalysts. As shown in Figure 3b, Pt nanoassemblies exhibited a mass activity of 12.4 A g^{-1} Pt at 0.85 V (versus a reversible hydrogen electrode (RHE)), which was about 1.5- and 2.1-times of that of commercial Pt and Pt/CB, respectively. Despite having a lower Pt ECSA than commercial Pt (Figure 3c), the specific ORR activity of Pt nanoassemblies was 2.2- and 1.7-times of that of commercial Pt and Pt/CB catalysts, respectively (Figure 3d). This improvement in activity agreed well with the results for Pt NWs.[13,18] Furthermore, an ORR durability test was carried out by accelerated cyclic voltammetry (CV). After 3000 cycles, the polarization curves of the commercial Pt catalyst showed a significant drop in the half-wave potential and an associated decrease in the diffusion-limited current (Figure 3e). On the contrary, Pt nanoassemblies showed only a slight decrease in the diffusion-limited current, and the half-wave potential remains almost unchanged over 3000 cycles (Figure 3f). It is therefore apparent that the Pt nanoassemblies possessed superior durability in terms of both ECSA retention and, more importantly, activity retention, when compared with the commercial Pt electrocatalyst.

The comparative electrocatalytic performances of the three Pt materials were further evaluated using the CV technique. First, the CV curves of the three catalysts were recorded at room temperature in a 0.5 M H_2SO_4 solution at a sweep rate of 100 mV s^{-1}. As shown in Figure 4a–c, all CV curves exhibited strong peaks associated with hydrogen adsorption/desorption (HAD) between −0.24 and 0.2 V, and Pt oxide formation/reduction in the range of 0.2–1.0 V. The ECSA was calculated by integrating the charge passing the electrode during the HAD, after correction for double-layer formation. The charge required to oxidize a hydrogen monolayer was measured as 0.21 mC cm^{-2}, which corresponded to a surface density of 1.3×10^{15} Pt atoms per cm^2. As shown in Figure 3c, the specific ECSA of Pt nanoassemblies was 40.8 m^2 g^{-1}, which was about 65% of that of the commercial E-TEK Pt catalyst (62.3 m^2 g^{-1}). The lower ECSA for the Pt-nanoassembly catalyst was most likely because of the large size of the Pt nanoassemblies (about 10 nm in diameter) compared with that of Pt nanoparticles (about 3 nm) in commercial catalysts. However, it was similar to that of Pt/CB (40.1 m^2 g^{-1}) because of the interconnected 3D hierarchical assembly and anisotropic NW building blocks, which can improve mass transport and catalyst utilization. The Pt nanoassemblies were also evaluated as an electrocatalyst for the methanol oxidation reaction (MOR), and exhibited improved catalytic activity and stability, as shown in CV and chronoamperometry (CA) curves (Supporting Information, Figure S6).

The durability of the electrocatalysts remains one of the most important issues to be addressed before the widespread application of fuel cells becomes feasible. Accelerated durability tests (ADT) of the catalysts were conducted by cycling the potential between −0.24 and 1.0 V in a 0.5 M H_2SO_4 solution at room temperature, for evaluation of the long-term electrochemical stability of the catalysts.[13,17,18] For

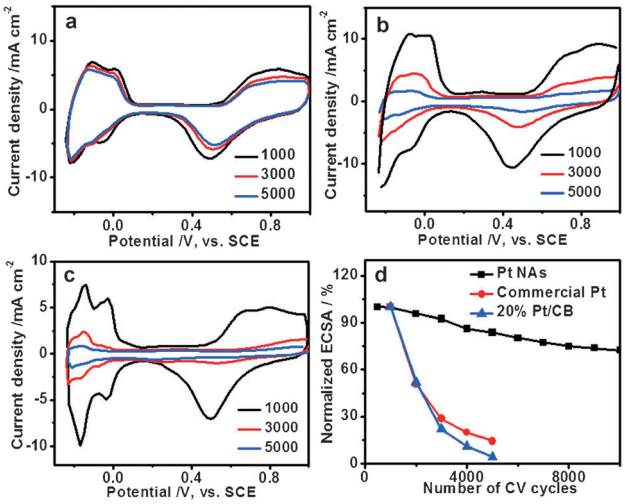

Figure 4. Comparison of the electrochemical durability of Pt nanoassemblies, commercial Pt catalysts (E-TEK), and self-prepared 20 wt% Pt/CB. Cyclic voltammetry (CV) curves for a) Pt nanoassemblies, b) commercial Pt catalyst, and c) Pt/CB catalyst after prolonged cycles of CV. The durability tests were carried out at room temperature in 0.5 M H_2SO_4 solution with a sweep rate of 100 mV s^{-1}. SCE = saturated calomel electrode. d) Loss of ECSA of Pt nanoassemblies (NAs), commercial Pt catalyst, Pt/CB catalyst with the number of CV cycles.

comparison, the stabilities of commercial Pt catalyst (E-TEK, 50 wt% Pt) and self-prepared 20 wt% Pt/CB were also studied under identical conditions. Figure 4a–c shows the CV curves of the three catalysts after 1000–5000 cycles. The current densities of the peaks in HAD potential region (−0.24–0.2 V) for the commercial Pt catalyst (Figure 4b) and Pt/CB (Figure 4c) dropped dramatically with the increase of the number of CV cycles. In contrast, the Pt nanoassemblies catalyst (Figure 4a) exhibited only a slight drop in the current densities of the peaks upon cycling in the same potential range. The loss of ECSA with cycling was plotted in Figure 4d. After 5000 cycles, the Pt nanoassembly catalyst lost only 16% of the initial Pt ECSA, while the commercial Pt and Pt/CB catalysts lost 85% and 95% of their initial ECSA, respectively. Even when the ADT test for self-supported Pt-nanoassembly catalysts was further prolonged to 10000 cycles, the ECSA only dropped about 27.5%. Moreover, in the CV profiles (Figure 4b,c), a decrease in the double-layer capacitance by about 75% for commercial Pt and Pt/CB catalysts was recorded after the Pt degradation test, which is related to the corrosion of the amorphous carbon support. However, no significant change in double-layer capacitance was recorded for Pt nanoassemblies owing to the absence of a carbon support. The ADT results demonstrated that Pt nanoassemblies have significantly higher stability than the commercial Pt and Pt/CB catalysts. To understand the loss of ECSA, a post-cyclization TEM investigation was carried out for the commercial Pt and Pt nanoassembly electrocatalysts (Supporting Information, Figure S7).

In summary, novel 3D Pt nanoassemblies consisting of 1D single-crystal Pt nanowires were prepared by a one-pot method. The presence of CTAB was found to be crucial for the formation of a 3D interconnected structure. The interconnected 3D Pt nanoassemblies showed a higher resistance to dissolution, migration, Ostwald ripening, and aggregation compared to the 0D Pt nanoparticles. Benefitting from unique structural features, these interconnected 3D Pt nanostructures, when evaluated as electrocatalysts for low-temperature fuel cells, manifest high electrochemical surface area and significantly improved long-term stability compared to the 0D Pt nanoparticles (commercial Pt catalyst and self-prepared Pt/CB nanoparticles catalyst).

Received: February 26, 2012
Published online: June 13, 2012

Keywords: cyclic voltammetry · electrocatalysts · fuel cells · nanowires · platinum

[1] R. F. Service, *Science* **2002**, *296*, 1222.
[2] R. Borup, J. Meyers, B. Pivovar, Y. S. Kim, R. Mukundan, N. Garland, D. Myers, M. Wilson, F. Garzon, D. Wood, P. Zelenay, K. More, K. Stroh, T. Zawodzinski, J. Boncella, J. E. McGrath, M. Inaba, K. Miyatake, M. Hori, K. Ota, Z. Ogumi, S. Miyata, A. Nishikata, Z. Siroma, Y. Uchimoto, K. Yasuda, K.-i. Kimijima, N. Iwashita, *Chem. Rev.* **2007**, *107*, 3904.
[3] B. C. H. Steele, A. Heinzel, *Nature* **2001**, *414*, 345.
[4] J. Zhang, K. Sasaki, E. Sutter, R. R. Adzic, *Science* **2007**, *315*, 220.
[5] Y. Bing, H. Liu, L. Zhang, D. Ghosh, J. Zhang, *Chem. Soc. Rev.* **2010**, *39*, 2184.
[6] X. Wang, W. Z. Li, Z. W. Chen, M. Waje, Y. S. Yan, *J. Power Sources* **2006**, *158*, 154.
[7] L. Cademartiri, G. A. Ozin, *Adv. Mater.* **2009**, *21*, 1013.
[8] Z. Xu, C. Shen, Y. Hou, H. Gao, S. Sun, *Chem. Mater.* **2009**, *21*, 1778.
[9] C. Koenigsmann, W.-p. Zhou, R. R. Adzic, E. Sutter, S. S. Wong, *Nano Lett.* **2010**, *10*, 2806.
[10] S. Maksimuk, S. Yang, Z. Peng, H. Yang, *J. Am. Chem. Soc.* **2007**, *129*, 8684.
[11] J. Mao, X. Cao, J. Zhen, H. Shao, H. Gu, J. Lu, J. Y. Ying, *J. Mater. Chem.* **2011**, *21*, 11478.
[12] T. Kijima, T. Yoshimura, M. Uota, T. Ikeda, D. Fujikawa, S. Mouri, S. Uoyama, *Angew. Chem.* **2004**, *116*, 230; *Angew. Chem. Int. Ed.* **2004**, *43*, 228.
[13] Z. Chen, M. Waje, W. Li, Y. Yan, *Angew. Chem.* **2007**, *119*, 4138; *Angew. Chem. Int. Ed.* **2007**, *46*, 4060.
[14] Y. Xia, P. Yang, Y. Sun, Y. Wu, B. Mayers, B. Gates, Y. Yin, F. Kim, H. Yan, *Adv. Mater.* **2003**, *15*, 353.
[15] H. Lee, S. E. Habas, S. Kweskin, D. Butcher, G. A. Somorjai, P. Yang, *Angew. Chem.* **2006**, *118*, 7988; *Angew. Chem. Int. Ed.* **2006**, *45*, 7824.
[16] T. K. Sau, A. L. Rogach, *Adv. Mater.* **2010**, *22*, 1781.
[17] Y. Liu, D. Li, S. Sun, *J. Mater. Chem.* **2011**, *21*, 12579.
[18] H.-W. Liang, X. Cao, F. Zhou, C.-H. Cui, W.-J. Zhang, S.-H. Yu, *Adv. Mater.* **2011**, *23*, 1467.
[19] D. Wang, H. Luo, R. Kou, M. P. Gil, S. Xiao, V. O. Golub, Z. Yang, C. J. Brinker, Y. Lu, *Angew. Chem.* **2004**, *116*, 6295; *Angew. Chem. Int. Ed.* **2004**, *43*, 6169.
[20] M. Rauber, I. Alber, S. Müller, R. Neumann, O. Picht, C. Roth, A. Schökel, M. E. Toimil-Molares, W. Ensinger, *Nano Lett.* **2011**, *11*, 2304.
[21] J. N. Tiwari, R. N. Tiwari, K. S. Kim, *Prog. Mater. Sci.* **2012**, *57*, 724.
[22] S. H. Sun, D. Q. Yang, D. Villers, G. X. Zhang, E. Sacher, J. P. Dodelet, *Adv. Mater.* **2008**, *20*, 571.
[23] E. P. Lee, J. Chen, Y. Yin, C. T. Campbell, Y. Xia, *Adv. Mater.* **2006**, *18*, 3271.
[24] J. H. Yuan, K. Wang, X. H. Xia, *Adv. Funct. Mater.* **2005**, *15*, 803.
[25] U. H. Lee, J. H. Lee, D. Y. Jung, Y. U. Kwon, *Adv. Mater.* **2006**, *18*, 2825.
[26] X. Zhang, W. Lu, J. Da, H. Wang, D. Zhao, P. A. Webley, *Chem. Commun.* **2009**, 195.
[27] M. J. Bierman, Y. K. A. Lau, A. V. Kvit, A. L. Schmitt, S. Jin, *Science* **2008**, *320*, 1060.
[28] A. Takai, H. Ataee-Esfahani, Y. Doi, M. Fuziwara, Y. Yamauchi, K. Kuroda, *Chem. Commun.* **2011**, *47*, 7701.
[29] V. Tzitzios, D. Niarchos, M. Gjoka, N. Boukos, D. Petridis, *J. Am. Chem. Soc.* **2005**, *127*, 13756.
[30] Y. Song, Y. Yang, C. J. Medforth, E. Pereira, A. K. Singh, H. Xu, Y. Jiang, C. J. Brinker, F. van Swol, J. A. Shelnutt, *J. Am. Chem. Soc.* **2004**, *126*, 635.
[31] T. K. Sau, A. L. Rogach, F. Jäckel, T. A. Klar, J. Feldmann, *Adv. Mater.* **2010**, *22*, 1805.
[32] A. Kloke, F. von Stetten, R. Zengerle, S. Kerzenmacher, *Adv. Mater.* **2011**, *23*, 4976.
[33] M. A. Mahmoud, C. E. Tabor, M. A. El-Sayed, Y. Ding, Z. L. Wang, *J. Am. Chem. Soc.* **2008**, *130*, 4590.
[34] Z. Niu, Q. Peng, M. Gong, H. Rong, Y. Li, *Angew. Chem.* **2011**, *123*, 6439; *Angew. Chem. Int. Ed.* **2011**, *50*, 6315.
[35] B. Lim, Y. Xia, *Angew. Chem.* **2011**, *123*, 78; *Angew. Chem. Int. Ed.* **2011**, *50*, 76.
[36] Y. Song, R. M. Garcia, R. M. Dorin, H. Wang, Y. Qiu, E. N. Coker, W. A. Steen, J. E. Miller, J. A. Shelnutt, *Nano Lett.* **2007**, *7*, 3650.

